Tuning the electronic effective mass in double-doped $SrTiO_3$

J. Ravichandran,[1,2] W. Siemons,[3] M. L. Scullin,[2,4] S. Mukerjee,[3,5] M. Huijben,[3,6] J. E. Moore,[2,3] A. Majumdar,[1,2,4,7] and R. Ramesh[2,3,4]

[1]*Applied Science and Technology Graduate Group, University of California, Berkeley, California 94720, USA*
[2]*Materials Sciences Division, Lawrence Berkeley National Laboratory, Berkeley, California 94720, USA*
[3]*Department of Physics, University of California, Berkeley, California 94720, USA*
[4]*Department of Materials Science and Engineering, University of California, Berkeley, California 94720, USA*
[5]*Department of Physics, Indian Institute of Science, Bangalore 560012, India*
[6]*Faculty of Science and Technology and MESA+ Institute for Nanotechnology, University of Twente, P.O. Box 217, NL-7500AE Enschede, The Netherlands*
[7]*Department of Mechanical Engineering, University of California, Berkeley, California 94720, USA*

(Received 27 April 2010; revised manuscript received 13 October 2010; published 4 January 2011)

We elucidate the relationship between effective mass and carrier concentration in an oxide semiconductor controlled by a double-doping mechanism. In this model oxide system, $Sr_{1-x}La_xTiO_{3-\delta}$, we can tune the effective mass ranging from 6 to $20m_e$ as a function of filling (carrier concentration) and the scattering mechanism, which are dependent on the chosen lanthanum- and oxygen-vacancy concentrations. The effective mass values were calculated from the Boltzmann transport equation using the measured transport properties of thin films of $Sr_{1-x}La_xTiO_{3-\delta}$. We show that the effective mass decreases with carrier concentration in this large-band-gap, low-mobility oxide, and this behavior is contrary to the traditional high-mobility, small-effective-mass semiconductors.

DOI: 10.1103/PhysRevB.83.035101 PACS number(s): 71.55.−i, 71.18.+y, 73.50.−h, 72.10.−d

I. INTRODUCTION

Variation of effective mass as a function of carrier concentration and temperature has been widely characterized in small-band-gap (0.1–1 eV) and low-effective-mass ($0.1–0.01m_e$) semiconductors[1] such as InAs,[2] HgTe,[3] and InSb.[4] Such systems show an increasing effective mass with carrier concentration and are sufficiently explained by Kane's band model, which captures the essential feature of nonparabolicity in these materials.[5] At the other end of the spectrum, complex oxides or transition metal oxides typically have larger effective masses ($1–10m_e$), large band gaps (1–10 eV), and conduction dominated by *d* bands. Complex oxides offer a variety of compounds showing no electron-electron correlation (band limit) to strong correlation (Mott limit). Strong correlations give rise to a very large effective mass ($100–1000m_e$) in heavy fermionic systems.[6] Even though the effect of strong correlation on effective mass and other transport properties remains an intriguing question, there is little literature on the study of effective mass as a function of a wide range of carrier concentration in transition-metal oxides in the band limit. Moreover, a thorough understanding and tuneability of effective mass in such oxide systems will have implications on phenomena such as thermoelectricity[7] and photovoltaics.[8]

In order to study the effective mass in the band limit, we have chosen $SrTiO_3$ (STO). STO is a model complex oxide system with very weak or no correlation and a wide range in *n*-type electrical conductivity, controlled by doping at the A site (for example, La doping in Sr sites) and B site (for example, Nb doping in Ti sites) and by creating oxygen vacancies. The cation doping on the A site of STO is more suitable than doping on the B site to study the nature of filling without changing the band structure drastically, because the conduction band has Ti 3*d* characteristics. The effective mass of La-doped STO has been reported as $6–6.6m_e$ in the literature,[9] and the introduction of oxygen vacancies, in lieu of La, results in a large effective mass of $\sim 16m_e$[10] and has been attributed to the flat impurity band created by these vacancies.[11] In this article, we explore the dependence of effective mass for double-doped STO on carrier concentration over a range of 3–4 orders of magnitude and show tuneability of the effective mass in the range $6–20m_e$. We also demonstrate that this behavior can be sufficiently explained using a single-parabolic-band model.

II. EXPERIMENTAL METHODS

Thin films (150 nm) of $Sr_{1-x}La_xTiO_{3-\delta}$ were grown via pulsed laser deposition (PLD) from dense polycrystalline, ceramic targets (each nominally containing either 0%, 2%, 5%, or 15% La) onto $(LaAlO_3)_{0.3}$-$(Sr_2AlTaO_6)_{0.7}$ (001) single-crystal substrates ($a = 3.872$ Å). Growth was carried out in oxygen partial pressures ranging from 10^{-1} to 10^{-7} Torr and a laser fluence of 1.75 J/cm^2 at a repetition rate of 8 Hz. Films were grown at a temperature of 450 °C to create a nonequilibrium amount of oxygen vacancies, by avoiding the equilibrium reached during the cool down from higher temperatures. X-ray diffraction (XRD) was carried out on these films with a Panalytical X'Pert Pro thin film diffractometer using Cu Kα radiation. Low-temperature resistivity and Hall measurements were performed using a Quantum Design physical property measurement system with magnetic field sweeps over a range of ±1.5 T. All measurements were carried out in van der Pauw geometry, and appropriate corrections were made to eliminate magnetoresistance contributions to the Hall resistance. Thermopower measurements at room temperature were done using a setup with T-type thermocouples. UV-Visible (UV-Vis) transmission, and reflection

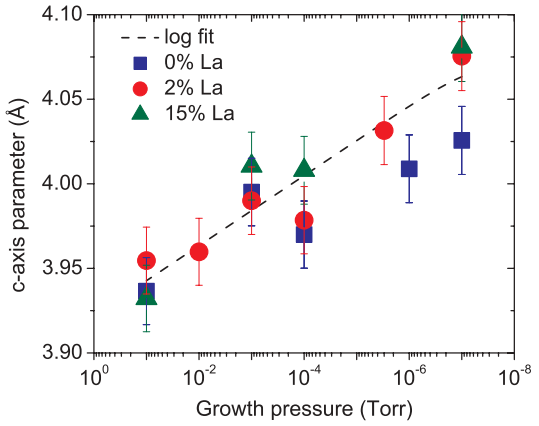

FIG. 1. (Color online) The c-axis lattice parameter measured by x-ray diffraction at 300 K vs. oxygen partial pressure during thin-film growth for $Sr_{1-x}La_xTiO_{3-\delta}$ (the dashed line is a logarithmic fit to the 2% data as a guide to the eye).

measurements were obtained from a Perkin Elmer Lambda 950 spectrometer and Hitachi U-3010 spectrometer, respectively. The photoluminescence (PL) data were acquired using a setup with a 325 nm laser excitation source. RBS measurements were carried out using a 2 MeV He ion beam generated by a 2.5 MeV Van de Graaff accelerator. The backscattered He ions were collected by a silicon surface-barrier detector located at 165° with respect to the incident beam.

III. RESULTS AND DISCUSSION

A. Structural and chemical characterizations

XRD patterns of the thin films indicated that they are single-phase perovskites. The narrow full-width-at-half-maximum (FWHM) of the rocking-curve (002) thin-film peaks indicate the films ($\omega_{002}^{\mathrm{FWHM}} < 0.3°$) are (00$l$) epitaxially oriented. The phi-pole scans (not shown here) were carried out along the (013) reflections to establish the in-plane epitaxial relationship between the film and substrate. A combination of out-of-plane texturing of the films and in-plane epitaxial relationship suggests a crystalline nature of the films. Typically, La doping has a negligible effect on the c-axis lattice parameter,[12] but oxygen vacancies will expand the lattice significantly as the Ti-Ti bond length is greater than that of Ti-O-Ti and induces a tetragonal distortion.[11,13] Reciprocal space mapping of the (013) peak of the thin films reveals they are indeed tetragonal, with an in-plane lattice parameter of ∼3.90 Å across all La concentrations and oxygen partial growth pressures, and a 0.023 Å increase in the c-axis lattice parameter per order of magnitude decrease in oxygen partial pressure during growth (Fig. 1). For samples grown at 10^{-7} Torr—or a maximum concentration of oxygen vacancies in our study—the c-axis lattice parameter is 4.075 Å for $Sr_{0.98}La_{0.02}TiO_{3-\delta}$,[14] corresponding to a c/a ratio of 1.045. RBS measurements were carried out to ensure the chemical homogeneity and stoichiometry of the films within the limits of the experimental accuracy of the technique. These measurements were crucial for reliable interpretation of the transport measurements and hence the effective mass calculations.

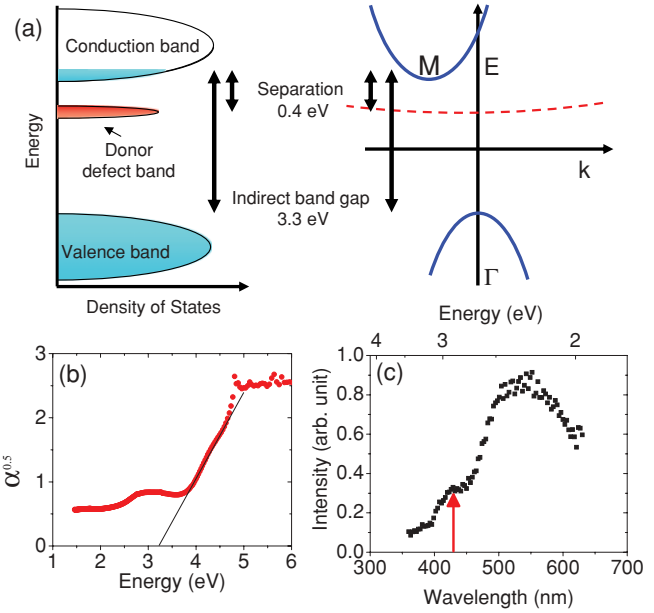

FIG. 2. (Color online) (a) Schematic of the band model for the oxygen-vacancy-doped La-STO. (b) Plot of square root of absorbance as a function of photon energy for UV-Vis absorption spectroscopy. The intercept of the linear part of the curve gives the indirect band-gap energy. (c) Plot of photoluminescence intensity as a function of energy. The red arrow indicates the peak position corresponding to the energy gap between the impurity level and the valence band. The data shown correspond to measurements at 300 K on 15% La-doped sample grown at 10^{-7} Torr.

B. Optical spectroscopy

The oxygen-vacancy-induced tetragonal distortion is expected to lift the threefold t_{2g} degeneracy of the conduction band. Theoretical predictions indicate that this leads to the formation of a heavy *oxygen-vacancy impurity band* lying below a light-conduction band edge.[11,15,16] In order to validate the predicted band model, schematically shown in Fig. 2, we performed UV-Vis spectroscopy and PL to map the important energy levels in the band model. UV-Vis spectroscopy was used to determine the energy gap between indirect conduction band and the valence band edges, and PL reveals the energy gap between the valence band edge and the oxygen-vacancy impurity band. Figure 2 shows the results obtained for a 15% La-doped sample grown at 10^{-7} Torr. The indirect band gap determined from UV-Vis was 3.3 eV, very close to the value observed in bulk STO 3.27 eV.[17] The PL spectra show a characteristic peak corresponding to ∼2.9 eV[18,19] suggesting a spacing of 0.4 eV between the indirect conduction band edge and the oxygen-vacancy impurity band as predicted by theoretical calculations.[11,15]

C. Transport measurements and effective mass calculation

Effective mass values have been conventionally evaluated using cyclotron resonance,[20] reflectivity,[21] photoemission,[22] and the Shubnikov-de Haas effect[23] for various single crystals of semiconductors. The other common method is using transport data to calculate the density of states' effective mass.[9,10] Some of these methods are impractical for thin films, and hence we resorted to calculating the density of states'

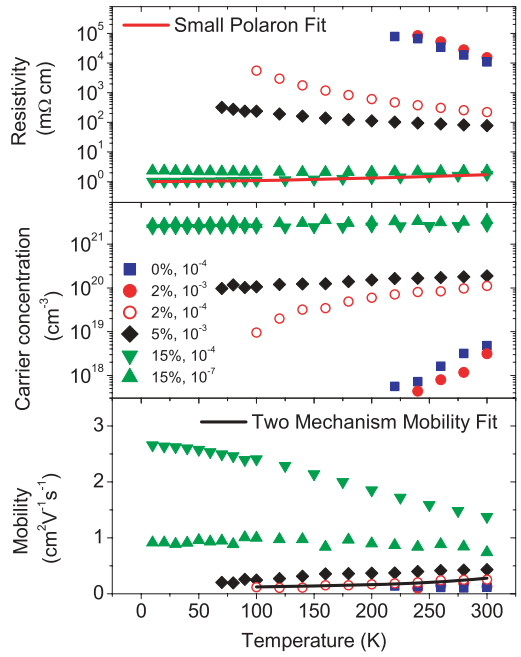

FIG. 3. (Color online) Low-temperature (top panel) resistivity, (middle) Hall carrier concentration, and (bottom) Hall mobility data for samples with different La doping and growth pressures (Torr). A representative two-mechanism mobility fit for a low-La-doping sample (2% La, grown at 10^{-4} Torr) and a small polaron fit for a high-La-doping sample (15% La, grown at 10^{-7} Torr) are also shown.

effective mass using transport data. All transport data were measured in the plane of the (00l)-oriented films. Evaluation of the effective mass at room temperature requires the knowledge of room-temperature thermopower S, low-temperature Hall mobility to learn about the scattering parameter r, and the carrier concentration n. Typical low-temperature resistivity, mobility, and carrier concentration data, which were used to derive these quantities, are shown for six representative samples in Fig. 3. The measured transport parameters for all the samples at room temperature are recorded in Table I.

The dominant scattering mechanism can be determined by the temperature dependence of the mobility. Typically, more than one scattering mechanism is present over the range of temperature under investigation. The samples containing low La doping (0%, 2%, or 5%) but with oxygen vacancies showed a constant mobility for temperatures near room temperature, indicating the presence of partially ionized impurity scattering or neutral impurity scattering[24] as the dominant scattering mechanism. In this limit, the transport is dominated by the oxygen vacancies, which ionize partially by localizing some of the electrons. In particular, clusters of oxygen vacancies can act as localizing sites for such itinerant electrons,[25,26] and clustering of vacancies is a common feature in PLD-grown STO thin films grown under low pressures.[27] In the case of samples containing 15% La, the low-temperature resistivity is best described by $\rho \sim \sinh^2(\frac{1}{T})$, characteristic of small polaron conduction. Recently, Liang *et al.*[28] suggested the possibility of small polaron conduction in 15% La-doped STO films grown under similar conditions, corroborating our observation. The optical phonon mode's characteristic temperature ($T_{\rm opt}$) derived by the fit was 100–120 K for the samples. It is interesting to note that this characteristic temperature is very close to the soft mode transition in $SrTiO_3$ at 110 K.[29] This indicates that the suitable scattering parameter for these samples at 300 K is $r = 1$ (for $T \ll T_{\rm opt}$, $r = \frac{1}{2}$ and $T \gg T_{\rm opt}$, $r = 1$).[30] Figure 3 shows the fit for both the conduction mechanisms in two representative samples.

With the known scattering mechanism, we can solve the Boltzmann transport equations. To simplify our calculations, we have modeled our system with an effective single parabolic band with effective mass m^*. The value of m^* was determined from the measurements of thermopower S and carrier concentration n (from the Hall mobility and resistivity). We have assumed that the presence of oxygen vacancies lifts the sixfold degeneracy, and hence the conduction band is only fourfold degenerate. The equations used for the model[24] are

$$S = \frac{-k_B}{e}\left[\frac{(r+2)F_{r+1}(\eta)}{(r+1)F_r(\eta)} - \eta\right], \tag{1}$$

$$n = 2\pi z\left(\frac{2m^*k_B}{T}h^2\right)^{\frac{3}{2}} F_{\frac{1}{2}}(\eta), \tag{2}$$

$$F_r(\eta) = \int_0^\infty \frac{x^r}{1+e^{x-\eta}}dx, \tag{3}$$

TABLE I. Various measured and derived physical quantities as a function of La doping and growth pressure in $Sr_{1-x}La_xTiO_{3-\delta}$ at 300 K; ρ is resistivity, n is Hall carrier density, μ is mobility, S is thermopower, r is scattering parameter, m^* is effective mass, m_e is electron mass, and η is reduced chemical potential (μ/k_BT).

La%	Growth pressure (Torr)	ρ (mΩ cm)	n ($\times 10^{21}$ cm^{-3})	μ cm^2 V^{-1} s^{-1}	S (μV/K)	r	$\frac{m^*}{m_e}$	η
0	10^{-4}	1.1×10^4	5×10^{-3}	0.12	−750	0.5	13.5	−6.2
0	10^{-7}	16.3	0.6	0.64	−274	0.5	8.3	−0.6
2	10^{-3}	1.5×10^4	3.1×10^{-3}	0.13	−832	0.5	18.6	−7.2
2	5×10^{-4}	1.4×10^3	1.8×10^{-2}	0.25	−572	0.5	9.2	−4.4
2	10^{-4}	220	0.12	0.26	−394	0.5	7.2	−2
2	10^{-7}	15.9	1.1	0.36	−190	0.5	7.1	0.6
5	10^{-3}	77.6	0.19	0.43	−313	0.5	5.6	−1.1
15	10^{-3}	4.6	2.1	0.65	−154	1	7.1	1.7
15	10^{-4}	1.7	2.7	1.36	−101	1	6.1	2.7
15	10^{-7}	2.7	3.1	0.75	−81	1	6.0	3.1

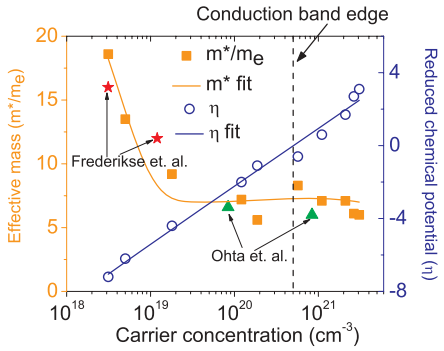

FIG. 4. (Color online) Calculated effective mass and reduced chemical potential in $Sr_{1-x}La_xTiO_{3-\delta}$ as a function of carrier concentration n at 300 K. Effective mass values from Ohta *et al.*[9] and Frederikse *et al.*[10] are also shown for reference. Fits are meant as a guide for the eye.

where k_B, h, e, η, z, r, and m^* are the Boltzmann constant, Planck's constant, electronic charge, reduced chemical potential (μ/k_BT), degeneracy of the conduction band, scattering parameter, and effective mass, respectively. The scattering parameter gives the energy dependence of the scattering time and is of the form $\tau(\epsilon) = \tau_0\epsilon^{r-\frac{1}{2}}$, where ϵ is the energy of the carrier. Knowing the scattering parameter from the temperature-dependent mobility data, we can solve Eqs. (1) and (2) to obtain η and m^*. All the measured and calculated values are listed in Table I.

The calculated values of the effective mass and reduced chemical potential as a function of carrier concentration are plotted in Fig. 4. The reduced chemical potential listed in Table I suggests that at low carrier concentration ($\sim 10^{18}$–10^{19} cm^{-3}) the samples are nondegenerately doped, and at higher carrier concentration ($\sim 10^{21}$) the doping tends toward the degenerate limit. At high doping levels ($\sim 10^{21}$), the chemical potential lies well inside the conduction band and shows a constant effective mass (~6–8). As the chemical potential moves well below the conduction band minimum, we see that the effective mass increases remarkably to high values (~14–18). Also, the effective mass decreases with increasing carrier concentration, unlike the conventional small-band-gap semiconductors, where the effective mass increases with increasing carrier density. This behavior is consistent with our assumption that STO should follow a simple filling-controlled parabolic band model, as has been observed in the past.[7,9]

IV. SUMMARY

In summary, we have measured the variation of effective mass as a function of carrier concentration in an n-type oxide semiconductor, through double doping with both an A-site dopant and oxygen vacancies in STO. The nature of m^* is mainly filling controlled in a parabolic band; specifically it decreases with increasing carrier concentration and can be tuned in the range of 6–20m_e by choosing a given doping combination. The tuneability in effective mass is achieved by the presence of a high-effective-mass impurity band that is separated from the conduction band by a small gap, as has been theorized prior to our observation of this energy level. A good understanding of the critical parameters may be used to better tailor the thermoelectric and photovoltaic response of oxide materials.

ACKNOWLEDGMENTS

The authors would like to acknowledge discussions with Choongho Yu, the assistance of Costel Rotundu and Kin Man Yu with Hall and RBS measurements, respectively, and the UC Berkeley/LBNL thermoelectrics group. W.S. acknowledges a Rubicon grant from The Netherlands Organization for Scientific Research (NWO). J.R. acknowledges a Link energy fellowship from the Link Foundation. This work was supported by the Division of Materials Sciences and Engineering, Office of Basic Energy Sciences, US Department of Energy under Contract No. DE-AC02-05CH11231.

[1] W. Zawadzki, Adv. Phys. **23**, 435 (1974).
[2] M. Cardona, Phys. Rev. **121**, 752 (1961).
[3] C. Verie and E. Decamps, Phys. Status Solidi **9**, 797 (1965).
[4] P. Byszewski, J. Kolodziejczak, and S. Zukotynski, Phys. Status Solidi **3**, 1880 (1963).
[5] E. O. Kane, J. Phys. Chem. Solids **1**, 249 (1957).
[6] G. R. Stewart, Rev. Mod. Phys. **56**, 755 (1984).
[7] T. Okuda, K. Nakanishi, S. Miyasaka, and Y. Tokura, Phys. Rev. B **63**, 113104 (2001).
[8] M. A. Green, Physica E **14**, 65 (2002).
[9] S. Ohta *et al.*, Appl. Phys. Lett. **87**, 092108 (2005).
[10] H. P. R. Frederikse and W. R. Hosler, Phys. Rev. **161**, 822 (1967).
[11] W. Luo, W. Duan, S. G. Louie, and M. L. Cohen, Phys. Rev. B **70**, 214109 (2004).
[12] J. E. Sunstrom IV *et al.*, Chem. Mater. **4**, 346 (1992).
[13] T. Zhao *et al.*, J. Appl. Phys. **87**, 7442 (2000).
[14] Since the sensitivity of techniques such as EELS, RBS, and EDS is only ~2% for impurity atoms and much higher for vacancies, characterization of the number of oxygen vacancies can be estimated only through measurement of n, and the precise relationship between oxygen growth pressure and δ is unknown.
[15] W. Wunderlich, H. Ohta, and K. Kuomoto, Physica B **404**, 2202 (2009).
[16] T. Tanaka, K. Matsunaga, Y. Ikuhara, and T. Yamamoto, Phys. Rev. B **68**, 205213 (2003).
[17] M. Capizzi and A. Frova, Phys. Rev. Lett. **25**, 1298 (1970).
[18] S. Mochizuki, F. Fujishiro, and S. Minami, J. Phys. Condens. Matter **17**, 923 (2005).
[19] D. Kan *et al.*, Nat. Mater. **4**, 816 (2005).
[20] G. Dresselhaus, A. F. Kip, and C. Kittel, Phys. Rev. **98**, 368 (1955).
[21] J. L. M. van Mechelen, D. van der Marel, C. Grimaldi, A. B. Kuzmenko, N. P. Armitage, N. Reyren, H. Hagemann, and I. I. Mazin, Phys. Rev. Lett. **100**, 226403 (2008).
[22] M. Takizawa, K. Maekawa, H. Wadati, T. Yoshida, A. Fujimori, H. Kumigashira, and M. Oshima, Phys. Rev. B **79**, 113103 (2009).
[23] H. P. R. Frederikse *et al.*, Phys. Rev. **158**, 775 (1967).

[24]C. B. Vining, J. Appl. Phys. **69**, 331 (1991).
[25]N. Shanthi and D. D. Sarma, Phys. Rev. B **57**, 2153 (1998).
[26]D. D. Cuong, B. Lee, K. M. Choi, H. S. Ahn, S. Han, and J. Lee, Phys. Rev. Lett. **98**, 115503 (2007).
[27]D. A. Muller *et al.*, Nature **430**, 657 (2004).
[28]S. Liang *et al.*, Solid State Commun. **148**, 386 (2008).
[29]P. A. Fleury, J. F. Scott, and J. M. Worlock, Phys. Rev. Lett. **21**, 16 (1968).
[30]B. M. Askerov, *Electronic Transport Phenomena in Semiconductors* (World Scientific, Singapore, 1994).